Advances in Science and Technology Research Journal

Advances in Science and Technology Research Journal, 2026, 20(2), 137–152
https://doi.org/10.12913/22998624/211588
ISSN 2299-8624, License CC-BY 4.0

Received: 2025.08.27
Accepted: 2025.11.15
Published: 2025.12.23

An innovative Maxwell-based thermo-viscoelastic framework for creep analysis in contact mechanics of nominally flat interfaces

AbdulJaleel H. Majeed[1], Osama M. Abuzeid[2], Safwan Al-qawabah[3*]

[1] Collage of Technical Engineering, Al-Farahidi University, Bagdad, 00965, Iraq
[2] School of Engineering, The University of Jordan, Amman, 11942, Jordan
[3] Faculty of Engineering and Technology- Al- Zaytoonah University of Jordan, Amman, Jordan
* Corresponding author's e-mail: safwan.q@zuj.edu.jo

ABSTRACT

The objective of this work was to formulate an analytical solution using generalized hypergeometric series to capture the thermo-mechanical response of a viscoelastic interface in contact with a rigid half-space across a nominally flat rough surface. The considered model sought to investigate the thermal creep of the rough surface as varied with the load applied and time. It is expected that the rough surface of the punch behaves like a Maxwell viscoelastic material. Given that real surface roughness was demonstrated to possess fractal characteristics, a deterministic Cantor structure representation was used to approximate such roughness. When the punch deflects throughout the size range of the roughness, an asymptotic power low in this model was found that links both the load and temperature of the punch to the creep of the asperity. Arrhenius' equation was used for establishing the connection between temperature and creep tendency. In the case of linear thermo-viscoelastic deformation, the suggested model allows for an analytical solution. The model's output closely matched the experimental findings that are publicly accessible through the literature.

Keywords: rough contact, creep, fractal, Maxwell viscoelastic model, confluent hypergeometric function, Arrhenius's equation.

INTRODUCTION

The tribological effectiveness of interfaces in contact may be improved by applying microlayers of compliant materials on them in many contact mechanics applications. Because such layers are finding more and more uses in industry, it is especially interesting to examine how their elastic characteristics differ from those of the substrate. Examples of this include viscoelastic load-bearing parts and sealing rubbers, and covering soft lubricants to hard surfaces in the automotive sector. The mechanical interaction among viscoelastic surfaces can be analyzed in a variety of ways, as suggested by the available literature. In [1], the authors applied Radok's method, which substitutes in the linear elastic model the congruent operators that show up in the constitutive viscoelastic materials, in an attempt to extend the effect of viscoelasticity to hertzian contact. The case of a rigid spherical indentation on a Maxwell and Voigt solid was studied in [2]. Since the stress-strain relations of the soft layer are rate dependent, it should be regarded as a viscoelastic material [3]. The conventional assumption in applied mathematics is that interacting viscoelastic bodies have topographically flat surfaces. Consequently, their interaction is nonexistent outside of the assigned contact area and continuous within it. Since the actual contact area is just a small portion of the actual contact zone as the contact is not continuous, this assumption excludes any real solids. No matter how smooth the surface is finished,

genuine viscoelastic solids always have some degree of waviness and roughness [4]. As a result, analyzing tribological issues, such as resistance to thermal and electrical contact, sealing, wear, and friction requires a precise description of the interaction among rough interfaces [5]. Some of the earliest theoretical models were stochastic [4, 6–8]. In these models, the surface topography appears to be random and statistical metrics are used to characterize surface roughness. Actually, the dimensionless statistical features of the rough interface used are not intrinsic characteristics of the surface; rather, they heavily rely on the measurement method, especially the surface finish, resolution of the measurement device and sample size [9]. One intriguing aspect of surface topography is that it exhibits irregularities across all scales, at least on the mesoscopic scale (a scale that sits between the microscopic and macroscopic levels).

Several studies [10–18] focus on developing or improving fractal-based models to describe the contact behavior of rough surfaces under normal loading. These works aim to capture elastic, plastic, or elastoplastic deformation by incorporating fractal geometry, asperity interactions, and multiscale effects to enhance predictions of contact area, load, stiffness, and deformation. In particular, [17] and [18] present fractal models for rigid-perfectly plastic and elastic-perfectly plastic contact, using Cantor set-based formulations to represent rough surfaces with greater mathematical rigor. References [19–21] explored the role of asperity size distributions and compared different modeling approaches – statistical vs. fractal—in predicting surface contact mechanics. Studies such as [22–24] examined broader implications of fractal characteristics: [22] highlighted the foundational importance of fractals in tribology; [23] analyzed the electrical response of fractal interfaces; and [24] investigates how fractal dimension and domain scaling affect contact models. Lastly, the study in [25] focused on modeling fractal contact spots and applied these concepts to improve the accuracy of isotropic rough surface contact predictions.

The relevance of surface fractality in determining mechanical response has been further emphasized in [26], where the fractal dimension was employed as a robust indicator of hardness in low carbon steels. This supports the adoption of fractal geometry to represent surface roughness in the current study, reinforcing the role of microscale topography in influencing creep and contact behavior at nominally flat interfaces.

Later investigations into the punch problem employed a range of linear viscoelastic constitutive laws to capture time-dependent material behavior. These encompassed creep responses of Maxwell [27], Kelvin-Voigt [28, 29], Jeffrey-type [30], and standard linear solid models [31], as well as relaxation phenomena described by Maxwell formulations [32] and thermally-influenced linear viscoelastic models [33]. In a recent study [34], a hereditary framework was developed to model the frictionless creep-contact behavior in a fractional viscoelastic material interfacing with a rigid substrate. The time-dependent constitutive response of the medium is described using the fractional-order Maxwell model, while the surface topography is characterized through fractal geometry to incorporate the influence of asperity-scale roughness. Recent studies have investigated the contact behavior between viscoelastic rough surfaces considering diverse loading scenarios and constraint conditions. The impact of friction when a rigid half space interacts with non-deterministic affine rough interface of a viscoelastic body was examined by [35], whereas [36] studied the sliding contact of rough viscoelastic solids. [37] investigated the rough surface contacts in elastic and viscoelastic thin layers. In [38], the rebound indentation response of a viscoelastic half-space indented by an axisymmetric punch was analyzed using the method of dimensionality reduction (MDR). A thorough investigation of the dampening of viscoelasticity in alternating contacts was presented by [39]. To examine the rough interaction between sliding layers of viscoelastic material, both theoretical and numerical investigations were carried out [40]. The work presented in reference [41] developed a model to analyze how viscoelasticity leads to anisotropic behavior in the contact of rough solids. Reference [42] focused on numerical simulations to evaluate the impact of creep on the relaxation of preload in composite joints fastened with bolts. A mathematical model for adhesive contact among viscoelastic stamps in printing processes was proposed in reference [43], offering insight into material behavior during stamping. The role of surface roughness in the indentation response of viscoelastic solids was further investigated by the authors in reference [44], highlighting its influence on deformation mechanics. Additionally, reference [45] introduced a novel incremental contact

model for viscoelastic rough surfaces, contributing to the understanding of time-dependent contact interactions. A data-driven hysteresis modeling approach using artificial neural networks was presented in [46], aimed at capturing the nonlinear, path-dependent response of viscoelastic materials under impact dynamics. While differing in methodology, this work shares common ground with the present study in addressing viscoelastic dissipation mechanisms, offering complementary insights into time-dependent contact behavior. A hereditary model for frictionless creep contact in a fractional viscoelastic medium was proposed in [47]. The constitutive behavior of a material is described by the fractional Maxwell model, capturing time-dependent and memory effects. Surface roughness is modeled using fractal geometry to reflect asperity interactions. This approach offers a more realistic representation of contact with rigid foundations.

Thermally induced creep is a critical consideration in engineering applications, particularly in the sectors where components are subjected to sustained mechanical stress at elevated temperatures. This time-dependent, thermally activated deformation mechanism can lead to dimensional instability and mechanical degradation in structural components, such as gears, frames, and support assemblies—ultimately compromising system efficiency and increasing maintenance demands.

In the aerospace industry, components like turbine blades and engine housings operate under extreme thermal and mechanical loads, making them highly susceptible to thermally induced creep, which can adversely impact performance, operational safety, and service life. Similarly, in the power generation sector, key components such as boiler tubes, steam turbine rotors, and high-temperature piping systems experience significant creep deformation over time, leading to reduced reliability and premature failure.

Automotive applications, especially the engines and transmissions operating under high load and thermal cycling conditions, also exhibit degradation due to creep phenomena. Moreover, in polymer-based systems such as seals and gaskets, thermally induced creep can result in relaxation, leakage, and mechanical failure under prolonged exposure to elevated temperatures and pressures.

Accounting for thermally induced creep during the design phase is essential to ensure the structural integrity, reliability, and longevity of engineering systems. A comprehensive understanding of time-dependent deformation behavior enables carrying out informed material selection, optimized component design, and accurate prediction of long-term performance.

In this work, an analytical model was developed to characterize the thermally induced creep behavior of a rough viscoelastic Maxwell body in contact with a rigid half-space under combined thermal and mechanical loading. Conceptually, the model introduced a fractal-based representation of surface roughness, allowing for a more realistic and scale-sensitive analysis of contact interactions. Methodologically, the formulation extends classical elastic contact solutions to the viscoelastic regime via the Radok correspondence principle, while incorporating thermo-viscoelastic coupling through the Arrhenius equation to relate creep behavior to activation energy. The resulting time-dependent solution, derived using Laplace transforms, reveals an asymptotic power-law relationship between punch displacement, applied load, and temperature. Parametric studies confirm the model's consistency with the experimental observations reported in the literature, thereby validating its predictive capability. These innovations distinguish the present framework from existing approaches and provide new insights into time-dependent contact behavior at nominally flat rough interfaces. The remainder of this paper details the model development, solution methodology, validation, and implications of the proposed framework.

FRACTAL CONTACT MODEL

The surface geometry considered in this study is based on the middle-third Cantor set, a classic example of a deterministic fractal structure. The surface topography is constructed under the assumption that the derived results are generalizable to all surfaces sharing the same fractal dimension. The contact mechanics of the interface are examined using this fractal configuration. The Cantor structure is generated by sequentially removing the central portion of each line segment at every iteration. The segments created at successive iterations are connected to form a multiscale, self-similar profile, as illustrated in Figure 1. At each construction stage, the total remaining segment length is equal to the original segment length multiplied by $1/a$, where a is a constant greater than 1.

In the $(i+1)^{th}$ iteration, the depth of the surface recesses is reduced by a factor of b, compared to the recess depth at the i^{th} stage, with $b > 1$. Using basic geometric relations, the horizontal length and recess depth for the $(i+1)^{th}$ iteration can be analytically determined based on the chosen values of a and b:

$$L_{i+1} = a^{-1}\ L_i = a^{-(i+1)} L_0 \tag{1}$$

$$h_{i+1} = b^{-1}\ h_i = b^{-(i+1)}\ h_0 \tag{2}$$

where: L_0 and h_0 are shown in Figure 1 and the surface profile is assumed to exhibit smoothness in the direction normal to the plane of the page. However, this assumption does not impose a significant constraint, as a surface profile oriented transversely to the page plane can also be constructed without loss of generality [10].

A practical method for determining whether the generated surface texture exhibits fractal characteristics is to evaluate its total length. The surface can be classified as fractal if the measured profile length satisfies the following condition:

$$L_{(i)} = L_0 + 2h_0\left(2b^{-(i+1)} - 1\right) / \left(2b^{-1} - 1\right) \tag{3}$$

when: through i successive iterations.

The surface profile exhibits fractal characteristics only when the scaling parameter $b \leq 2$, as in this case, the total contour length diverges toward infinity. It is well established that most engineering rough surfaces display self-affine scaling, meaning their geometric features scale differently along different directions [48]. This behavior is exemplified by the Cantor structure shown in Figure 1.

The surface trace in Figure 1 can be viewed as a discrete step-function representation. Analysis shows that the vertical fluctuation between successive iterations follows the scaling law $\Delta z_{i+1} = (a\,b)^{-1}\Delta z_i$, where $\Delta z(x)$ represents the trace of a fractional Brownian motion. The corresponding horizontal scaling is given by $\Delta x_{i+1} = (2\,a)^{-1}\Delta x_i$, with each step representing a stage in the recursive surface construction. The probability of obtaining a surface height z_i at the ith iteration is expressed as $\Delta z_i \propto z_i P(z_i)$, where $z_i = h_0 / b^i$ and the associated probability distribution is $P(z_i) = (1 - a^{-1})\,a^{-i}$. The well-known Hurst exponent H defines the scaling relationship between the standard fluctuation in surface height $\Delta z(x)$ and the change in spatial coordinate Δx, such that $\Delta z(x) \propto \Delta x^H$ [49].

Applying this scaling yields the relationship $(2a)^H = ab$, which corresponds to the result obtained by [10], from which

$$H = \frac{\ln(a\,b)}{\ln(2\,a)} \tag{4}$$

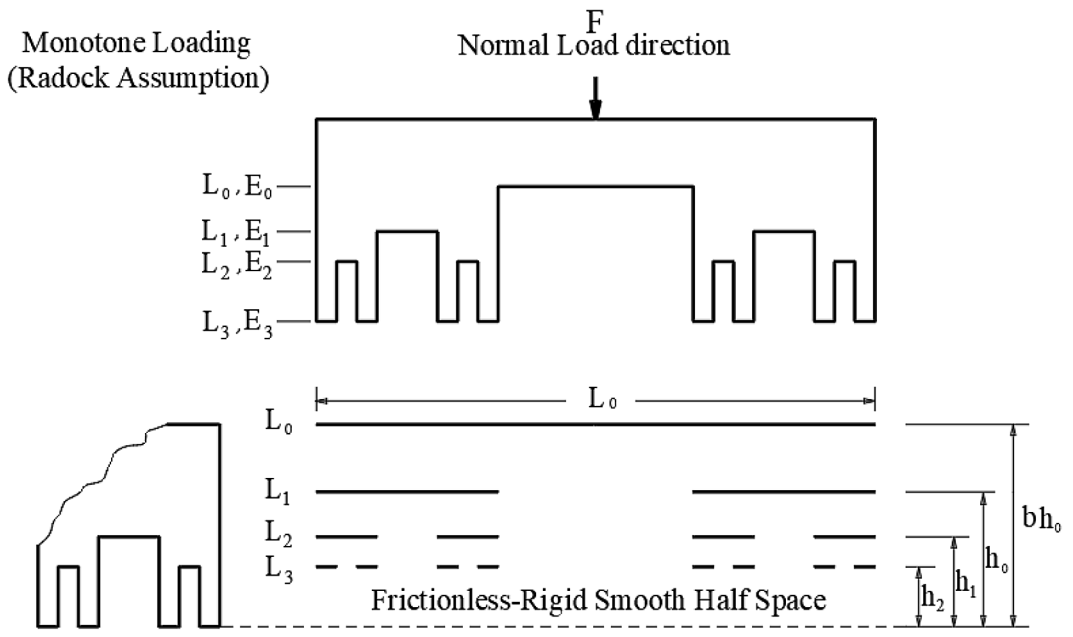

Figure 1. The fractal Cantor punch structure generated using (a=3/2), together with a schematic of the loading configuration. A rigid smooth half-space is indented by the fractal punch under normal loading, assuming frictionless contact and monotonic loading in accordance with Radok's correspondence principle

The self-affine fractal dimension characterizing the contour geometry of the Cantor-type structure is determined using the following relation

$$D = 2 - H \tag{5}$$

In this context, D denotes the fractal dimension of the surface-treated profile, providing a quantitative measure of its roughness or complexity.

VISCOELASTIC MODEL IN CONTINUOUS FORM

According to the classical contact mechanics framework [50], the contact problem can be qualitatively described by two distinct length scales. The first corresponds to the macroscopic (nominal) contact dimensions, where the stress distribution and deformation can be approximated using Hertzian contact theory. The second scale pertains to the microscale distribution of surface asperities. At each point within the nominal contact region, the theoretical contact pressure increases with applied load, while the real contact area evolves proportionally due to the progressive engagement of asperities. Assuming the contacting surface behaves as a viscoelastic foundation, the asperities act as a compliant interfacial layer, effectively extending the range of actual contact, compared to an idealized smooth interface. As a result, deformation is localized within a finite surface zone, denoted by $b\,h_0$ in Figure 1, representing the effective height or influence zone of individual asperities. The most direct approach to addressing this problem involves the application of Radok's method [49], which provides a framework for evaluating stress and deformation in viscoelastic materials by utilizing known solutions from linear elasticity. As stated in [2], Radok's method is valid for contact problems under monotonically increasing contact area, i.e., when the loading history is such that the contact region expands without reduction.

Referring to Figure 1, a discrete system composed of an array of independent, linearly elastic columns was considered. The vertical displacement steps are defined as follows: the distance between step E_0 and E_3 is h_0, between E_1 to E_3 is h_1, between E_2 to E_3 is h_2, and so on [10].

By sequentially applying compressive forces, the corresponding contact forces required to bring successive steps into engagement are: F_3 to compress E_3 to the level of E_2, F_2 to bring E_3 and E_2 to E_1, and F_1 to compress all elements down to E_0. Thus

$$\Delta F_{i+1} = E\,L_0\left(b-1\right)b^{-(i+1)}a^{-i} \tag{6}$$

The force F_{i+1} is expected to correspond to the upper limit of the load required to form the $(i+1)^{th}$ protrusion in the current forming sequence. Typically, the punch advances by a displacement Δu_{i+1}, which reflects the difference in protrusion heights between the i^{th} and $(i+1)^{th}$ *sta*ges, once the optimal forming load has been reached.

Assuming the elastic deflections of the forming stages—denoted as E_2, E_1 and E_0 — are represented by the respective punch displacements $u_2 = h_1$, $u_1 = h_0$, and $u_0 = bh_0$, the incremental punch displacements between successive stages can be expressed as: $\Delta u_1 = u_0 - u_1 = h_0(b-1)$, $\Delta u_2 = u_1 - u_2 = h_0 b^{-1}(b-1)$. Accordingly:

$$\Delta u_{i+1} = h_0\left(b-1\right)b^{-i} \tag{7}$$

The previously stated assumptions are sufficient to determine the influence of the punch displacement u on the limit forming load F. Specifically, the fact that the punch advances by a defined increment Δu_{i+1} as the forming load increases from F_{i+1} to F_i will be utilized to evaluate the remote or distant-load effect:

$$\frac{\Delta F_{i+1}}{\Delta u_{i+1}} = \frac{E\,L_0}{b\,h_0}\,a^{-i} \tag{8}$$

The following asymptotic behavior will be approached in the limit as the stage index $i \to \infty$, representing the steady-state condition of the forming process

$$\frac{u}{h_0} = \left(\frac{\chi\, b}{E}\frac{F}{L_0}\right)^{\frac{1}{\chi+1}} \tag{9}$$

where: $\chi = \ln a / \ln b$. It should be noted that these models are also constrained by a limiting load condition, defined as $F = \sigma_y\, L_0$, where σ_y is the material yield stress and L_0 is a characteristic length parameter.

EFFECT OF TEMPERATURE

The relationship between temperature and time in certain viscoelastic materials can be explained by correspondingly straightforward models. These materials are referred to as "thermorheologically simple." When the temperature is lowered for these

simple materials, the viscoelastic behavior simply shifts rightward (leftward) keeping the shape and the creep modulus reserved, while the creep time τ is increased (decreased).

The term time-temperature shift factor (a_T) refers to the horizontal offset needed to transfer the response curve recorded at whatever temperature T to the curve obtained at reference value T_{ref}. As demonstrated by [50], the shift factor can be determined via Arrhenius relation as:

$$\log a_T = \frac{Q}{2.303R}\left(\frac{1}{T} - \frac{1}{T_{ref}}\right) \tag{10}$$

where: T is the temperature (Kelvin), R is the universal gas constant (J/molK), and Q is the activation energy (kJ), independent of the temperature.

ARRHENIUS'S FORMULA

Usually, one may utilize the creep dependency on applied load, time, and temperature to characterize the creep properties of materials as:

$$\varepsilon = f(\sigma, t, T) \tag{11}$$

According to [53], the division of this formula into three separate functions as shown helps simplify it:

$$\varepsilon = f_1(\sigma) f_2(t) f_3(T) \tag{12}$$

The creep of materials is significantly influenced by temperature. According to [54], temperature has a more noticeable impact on some steels than strain rate.

A heated body may experience thermal forces and deflections due to external constraints or an uneven temperature distribution. It is assumed that the issue is one of steady state, meaning there is no internal heat. According to [51], the Arrhenius law provides a straightforward, yet remarkably accurate formula for the temperature dependence:

$$f_3(T) = B\exp\left(\frac{Q}{RT}\right) \tag{13}$$

which denotes the ideal gas constant (R), the activation energy (Q), and a constant (B). $f_1(\sigma) f_2(t)$ will be revealed afterwards.

In the experiment conducted in [55], the authors employed 0.45% carbon steel, which is classified as medium carbon steel. The study in [53] examined the influence of temperature, strain, and carbon content on the mechanical behavior of steels. Their findings indicate that activation energy varies with temperature and strain rate but remains largely unaffected by the carbon content. For this work, an activation energy value of Q=7 kJ/mol is adopted. According to the results reported in [53], this activation energy is valid for medium carbon steel within the temperature range of 298 to 1073 K. It can be directly demonstrated from Equation 13 that the value of the constant B at the reference temperature T_0 is:

$$B = \exp\left(\frac{-Q}{RT_0}\right) \tag{14}$$

ELASTIC-VISCOELASTIC CORRELATION

Creep or relaxation functions are used to characterise the viscoelastic material properties, which account for the time-dependent behavior of the material. This method works in circumstances where the strain is minimal. To explain the viscoelastic behavior of the material, Maxwell medium is utilized. As it can be seen in Figure 2, the linear spring (storing energy element) and the dashpot (dissipating energy element) in this model are grouped in series, in which E represents the Young's modulus and η represents the Newtonian viscosity. Applying the linear differential time operator, the following form might be used to describe the time, force, and displacement relation [56]:

$$\left\{\partial_t / E + 1/\eta\right\} F = \left\{\partial_t\right\} u \tag{15}$$

where: $\partial_t \equiv \partial / \partial t$ is the linear differential time operator.

Fundamentally, the preceding expression constitutes the one-dimensional form of the constitutive relation of the material. It is important to note that this relation no longer describes a simple linear proportionality between load and displacement, as it now includes time-dependent (temporal) derivatives. As discussed in [55], the viscoelastic modifier associated with the elastic modulus E in Equation 8 can be represented as follows:

$$\frac{1}{E} \to \frac{1}{E}\frac{\partial_t + 1/\tau}{\partial_t} \tag{16}$$

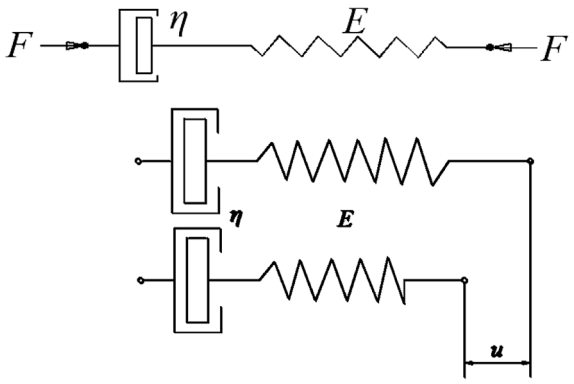

Figure 2. Maxwell model with linear viscoelastic properties

In this context, the retardation time, $\tau \equiv \eta / E$, is a characteristic time-dependent parameter that quantifies the delay in strain response under loading.

The present formulation employs *Radok's correspondence principle* to generalize elastic contact solutions to viscoelastic materials. Its validity is restricted to the cases of monotonically increasing contact area, as shown by Radok [51], since the convolution-based hereditary operators break down under unloading or contact reduction. Accordingly, the analysis assumes continuous, non-reversing loading with a growing contact region. The situations involving unloading, cyclic, or non-monotonic loading require alternative approaches (e.g., Ting's extension [58]) and are not considered here.

Linear viscoelastic behavior can typically be characterized using either a creep compliance model or a stress relaxation model. In the present analysis, a creep-based formulation was employed. To evaluate the time-dependent displacement (or indentation depth), a creep test was considered, in which a constant load F_0 was instantaneously applied to the viscoelastic material and maintained thereafter.

$$F = F_0 [U(t)] \tag{17}$$

where: $[U(t)]$ denotes the unit step function, applied at time $t = 0$ to represent the instantaneous application of load.

By utilizing standard Laplace transform tables [59], and substituting Equations 15, 16, and 17 into the constitutive relation given by Equation 9, the following expression was obtained:

$$f_1(\sigma) f_2(t) = \left(\frac{u(t)}{h_0} \right)_1 = \left(\frac{b}{E} \frac{\chi}{} \frac{F_0}{L_0} \right)^{\frac{1}{\chi+1}} e^{-t/\tau} \times {}_1F_1 \left[\frac{2+\chi}{1+\chi} ; 1; \frac{t}{\tau} \right] \tag{18}$$

where: ${}_1F_1[2+\chi/1+\chi; 1; t/\tau]$ is the confluent hypergeometric function called Kummer's equation, can be stated as follows [60]:

$${}_1F_1[c; d; x] = 1 + \frac{c}{d} x + \frac{c(c+1)x^2}{d(d+1)2!} + \frac{c(c+1)(c+2)x^3}{d(d+1)(d+2)3!} + \cdots \tag{19}$$

$$\text{or} \quad {}_1F_1[c; d; x] = \sum_{n=0}^{\infty} \frac{(c)_n}{(d)_n} \frac{x^n}{n!} \tag{20}$$

Finally, the creep behavior was estimated to be after rearranging the value of constant B using Equation 14 in Equation 13, as well as shifts in Equations 9 and 13 into Equation 12:

$$\varepsilon = \frac{u(t)}{h_0} = f_1(\sigma) f_2(t) f_3(T), \text{ or}$$

$$\frac{u(t)}{h_0} = \left(\frac{b}{E} \frac{\chi}{} \frac{F_0}{L_0} \right)^{\frac{1}{\chi+1}} e^{-t/\tau} \times {}_1F_1 \left[\frac{2+\chi}{1+\chi} ; 1; \frac{t}{\tau} \right] \times \exp\left(\frac{Q}{R} \left(\frac{1}{T} - \frac{1}{T_0} \right) \right) \tag{21}$$

The hypergeometric series in Equation 21 was truncated after $N = 500$ terms; truncation error was estimated from the ratio of successive terms and found to be $<10^{-9}$ over the plotted parameter range.

RESULTS AND DISCUSSION

This study focused on the analytical solution derived in Equation 21, which constitutes a novel closed-form expression describing the time-dependent creep behavior of a thermo-viscoelastic contact system. The surface roughness was modeled using a Cantor-type fractal geometry to capture the multiscale characteristics of real material interfaces. To facilitate the implementation of this model, the following assumptions were adopted:

1. A Winkler foundation is used to model the cantor surface of Figure 1.
2. The two contacting interfaces are represented as a single, identical rough surface contacting a rigid, smooth interface.
3. Radok's method, which substitutes in the linear elastic model the congruent operators that show up in the constitutive viscoelastic materials,
4. It is considered that the activation energy remains constant throughout the entire temperature range.

This model requires four different types of numerical values to be used:

1) Geometric parameters of the surface topography: The fractal characteristics of the rough surface are defined by the fractal dimension D and scaling parameters a and b. The geometry is based on the middle-third Cantor set. Fixing $a = 1.5$ yields a dimension $D = 0.63093$ as derived by [48]. Two distinct surface profiles are considered by varying parameter b, resulting in fractal dimensions $D = 1.5$ for $b = 1.155$ and $D = 1.24$ for $b = 1.54$, respectively.
2) Material parameters, specifically the dynamic viscosity η (MPa·s) and the elastic modulus E (MPa), play a critical role in the characterization of viscoelastic behavior. For a Maxwell material to appropriately represent a solid-like response—as opposed to fluid-like behavior—the viscosity η must be sufficiently large relative to the elastic modulus E, such that the characteristic relaxation time $\tau \equiv \eta / E \cong 1$ (in units of time) reflects delayed deformation under load. To ensure the model provides an accurate fit to experimental data for various viscoelastic materials, these parameters must be selected judiciously. As the Maxwell model is an idealized construct – comprising a linear spring and dashpot connected in series – the values of η and E should be tuned to reflect the material response relevant to the specific application, rather than treated as intrinsic, fixed material constants.
3) Experimentally determined quantities, such as h_0 and Q. Experimental validation of the Greenwood and Williamson contact model was accomplished by [55]. Carbon steel specimens (0.45 percent carbon) that had been face-turned, ground, and bead-blasted were used in the experiments. These specimens came into touch with a stiff, smooth ones. It was established that the displacement and load experimental measurements had an approximation error. According to [53], twice the r.m.s height corresponds to 9.7 μm, which was chosen as the depth h_0. The ideal gas constant, R, will be $8.314(10^{-3})$ kJ/K.mol, and the activation energy, Q, will be 7 kJ/mol. The model was validated using a range of temperature values.
4) Emperical variable. The quantity assigned to n in Equation 20 needs to be sufficiently large for the outcome to approach a steady value; this implies that $n > 500$ numerically.

The resulting model incorporates the previously defined material and system parameters. Subsequently, its predictions were compared against the experimental results reported in [53] for medium carbon steel specimens exhibiting different surface roughness levels due to various machining and finishing processes. The subsequent figures provide graphical representations of the analytical creep response for a range of system parameters. The thermo-viscoelastic creep strain, u / h_0 , represented by Equation 21, is graphed in opposition to the normalized time values, t / τ , in Figure 3. To evaluate the performance of the proposed model, two distinct fractal dimensions-1.24 and 1.5- were considered, along with two externally applied uniaxial stresses of 100 MPa and 150 MPa. The temperature in this figure is isothermal, or $\Delta T = 0$.

As expected from classical creep behavior, higher applied stresses result in increased strain rates. Selected analytical results related to thermally activated creep are presented graphically in the following figures, illustrating the influence of various system parameters. The plot clearly demonstrates that increasing the fractal dimension leads to elevated creep strain rates. This observation reflects the effect of surface roughness: lower fractal dimensions (e.g., D = 1.24) correspond to smoother surfaces, where bulk material deformation governs the creep response; conversely, higher fractal dimensions (e.g., D = 1.5) represent rougher contact surfaces, where localized deformation at surface asperities becomes more pronounced. Figures 4 and 5 illustrate the strain–time behavior of the material under a constant external creep load, considering variations in fractal dimension and temperature. Consistent with the established creep theory, an increase in temperature leads to a higher creep strain, indicating enhanced thermally activated deformation mechanisms.

The structural response under loading, in terms of load versus deflection, is shown in Figures 6 and 7 for various normalized time ratio t / τ , also referred to as isochronous curves when compared to the experimental findings. This kind of representation can be thought of as a fairly useful tool for predicting the behaviour of the material at various ambient temperatures. The load validity is limited to the situations where the contact area increases monotonically; as demonstrated by Radok [51], the analysis presumes continuous, non-reversing loading with an expanding contact region.

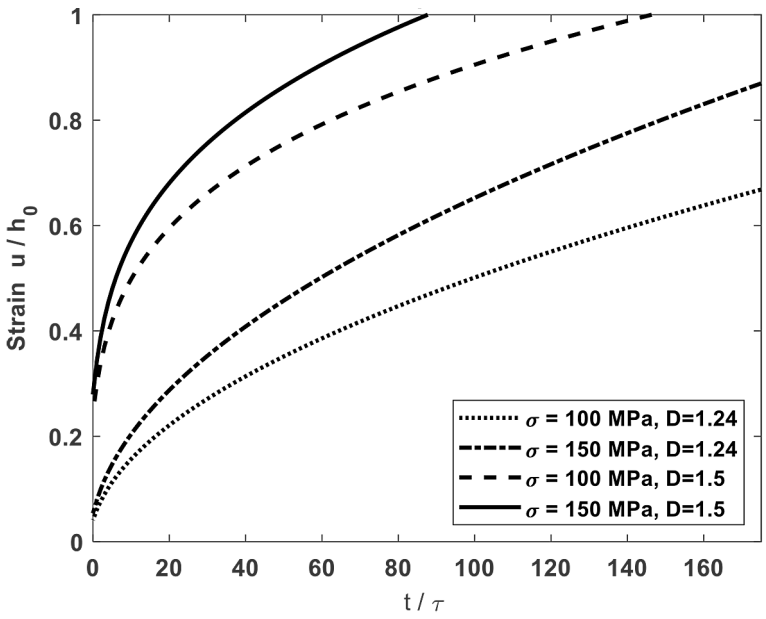

Figure 3. Curves representing strain-time for various external creep loads and fractal dimensions

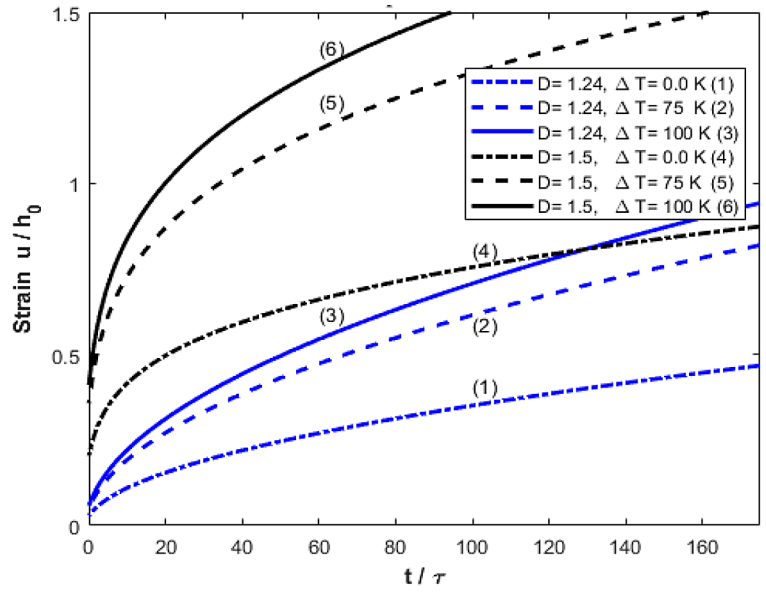

Figure 4. Strain-time curves for a constant creep stress (σ = 150 MPa), various fractal dimensions, and various temperatures

To ensure accurate correlation between the model predictions and experimental results, the normalized time period, t/τ ($\tau \equiv \eta/E$), must vary between 10 and 40 for D = 1.5 and between 100 and 200 for D = 1.24 in order to achieve a reasonable agreement among the experimental results as compared with the isochronous curves. Such values only serve the goal of the modeling process and are purely nominal. It is well established that metallic creep behavior typically progresses through three stages – primary (transient), secondary (steady-state), and tertiary (accelerating). The present study focused primarily on capturing the primary and secondary stages of creep deformation. To evaluate the robustness of the proposed model and understand the role of thermal effects, a sensitivity analysis with respect to temperature was performed. This approach assesses how changes in temperature influence the viscoelastic creep response, particularly through the Arrhenius-type dependence of the relaxation time. The analysis provides insights into the model's physical

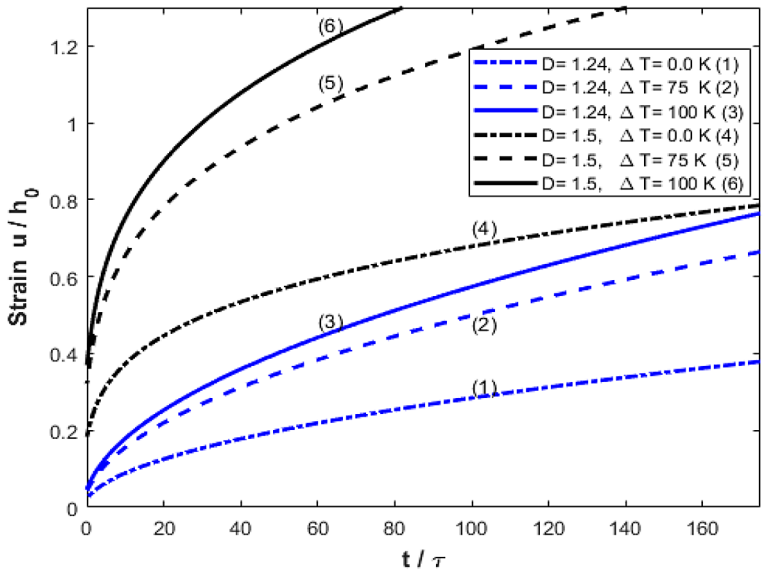

Figure 5. Strain-time curves for a constant creep stress (σ = 100 MPa), various fractal dimensions, and various temperatures

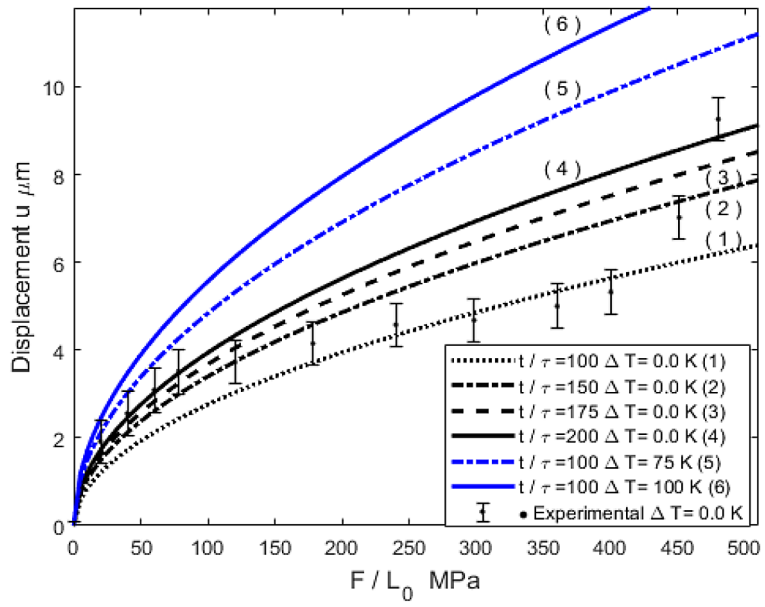

Figure 6. Isochronous load–displacement curves for fractal dimension D = 1.24 at various temperature differences, together with experimental data for carbon steel specimens (0.45% C) prepared by face-turning, grinding, and bead-blasting. The dataset, with twice the r.m.s. surface roughness of 9.7 μm, was obtained by Handzel-Powierza et al. at room temperature

consistency and its predictive behavior across a range of realistic thermal conditions.

Sensitivity analysis with respect to temperature

To evaluate the influence of temperature on the proposed viscoelastic contact model, a systematic sensitivity analysis was conducted. The analysis focused on how variations in temperature T affect key aspects of the model, including creep behavior, thermal activation mechanisms, and load–displacement–time relationships.

Temperature-dependent mechanisms

The model accounts for thermal effects through thermo-viscoelastic coupling, implemented via

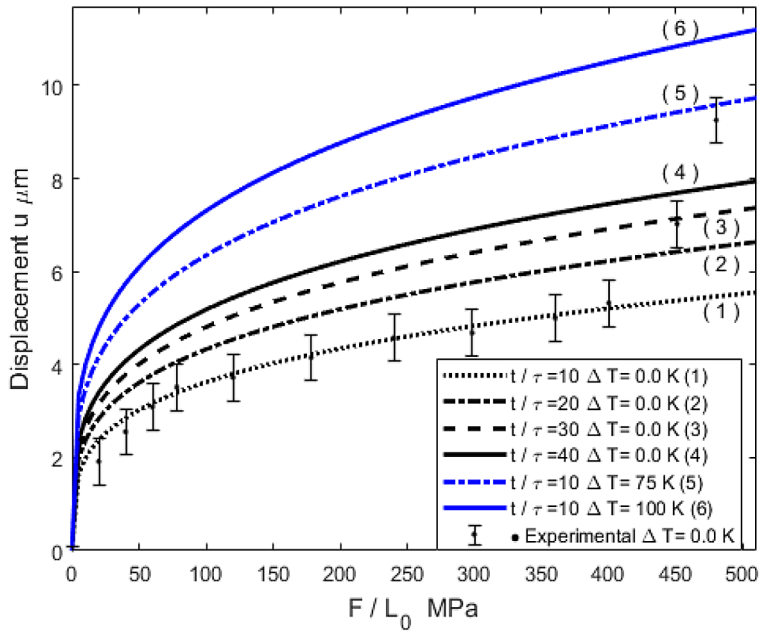

Figure 7. Isochronous load–displacement curves for fractal dimension $D = 1.5$ at various temperature differences, together with experimental data for carbon steel specimens (0.45% C) prepared by face-turning, grinding, and bead-blasting. The dataset, with twice the r.m.s. surface roughness of 9.7 μm, was obtained by Handzel-Powierza et al. at room temperature

a temperature-dependent relaxation time. This is governed by the Arrhenius-type relation:

$$\tau(T) = \tau_0 exp\left(\frac{Q}{RT}\right) \tag{22}$$

where: τ_0 is the reference relaxation time, Q is the activation energy, R is the ideal gas constant, and T is the absolute temperature in kelvins.

This relation reflects the fact that as temperature increases, the relaxation time $\tau(T)$ decreases exponentially. In the context of viscoelasticity, this means that the material creeps more quickly at higher temperatures under constant load. Consequently, the time scale of creep is temperature-dependent: higher temperatures lead to faster deformation rates. The effective stiffness and damping of the viscoelastic response (modeled via Maxwell elements) are also affected, since they depend on the relaxation dynamics governed by $\tau(T)$.

Simulation setup

To study the impact of temperature variations, the model was simulated at three temperature levels: T_0, T_0+75 K, T_0+100 K, at two stress levels: σ = 100 MPa, and σ = 150 MPa, and two fractal dimensions: $D = 1.24$, and $D = 1.5$.

Results and interpretation

The creep response is characterized by the normalized displacement u / h_0 as a function of normalized time t / τ. The key findings are summarized as follows:

- Temperature accelerates creep: At higher temperatures, the material deforms more rapidly and reaches greater displacements.
- Fractal roughness amplifies thermal effects: Larger fractal dimensions (e.g., $D = 1.5$) result in greater sensitivity to temperature changes.
- Stress scales the response: Higher applied stress increases the magnitude of creep deformation, though the qualitative temperature trends remain consistent.

The Power-law behavior is preserved: The strain-time relationship follows:

$$\frac{u(t)}{h_0} = \left(\frac{b\,\chi}{E}\frac{F_0}{L_0}\right)^{\frac{1}{\chi+1}} e^{-t/\tau} \times$$

$$\times\, {}_1F_1\left[\frac{2+\chi}{1+\chi};1;\frac{t}{\tau}\right] \times \exp\left(\frac{Q}{R}\left(\frac{1}{T}-\frac{1}{T_0}\right)\right)$$

repeated (21)

Figures 4 and 5 illustrate these behaviors clearly, showing how increasing temperature shifts the curves upward and to the left, indicating faster and larger creep deformation. For example, under the same load:

- At $T = 400\,\mathrm{K}$, the predicted displacement is approximately 2.5× greater than at $T = 250\,\mathrm{K}$.
- This highlights the significant role of temperature in accelerating viscoelastic creep, consistent with the exponential dependence of $\tau(T)$.

These results confirm that the model reliably captures thermally activated viscoelastic creep, and is capable of describing coupled effects involving temperature, surface roughness, and loading history.

Parameter identification protocol

The temperature-dependent parameters used in the model were identified as follows:

- activation energy Q=7 kJ/mol and
- reference relaxation time τ_0

were selected based on available literature values typical for viscoelastic materials. In the absence of specific experimental data for the material system in question, physically reasonable estimates were adopted. Their influence was explored through the sensitivity analysis presented here, confirming the model's robustness to variations in these parameters. To situate the present framework within the broader literature, it is useful to compare it with representative contact models. Classical viscoelastic formulations, pioneered by Lee and Radok [2] and Hunter [61], extended elastic contact theory to linear viscoelastic solids but are valid only under isothermal, monotonic loading. Later thermo-viscoelastic approaches, such as those of He et al. [62] for polymeric interfaces and Zhang et al. [63] for layered materials, incorporated temperature dependence, yet often assumed simplified geometries and did not fully capture rough-surface effects. In parallel, fractal and rough-surface models—including Majumdar and Bhushan [15], Persson [64], and Ciavarella et al. [65] – successfully described multiscale morphology as well as its role in stiffness and real contact area, but were largely

Table 1. Comparison between the proposed model and representative categories of existing approaches in contact mechanics, highlighting the novelty and scope of the present work

Feature	Classical Viscoelastic Contact Models (Lee and Radok [2]; Hunter [61])	Thermo-Viscoelastic Contact Models (He et al. [62]; Zhang et al. [63])	Fractal Rough Surface Models (Majumdar and Bhushan [15]; Persson [64]; Ciavarella et al. [65])	Present work
Material model	Linear viscoelastic (spring–dashpot, SLS, fractional)	Thermo-dependent viscoelastic (polymers, TVEHL)	Elastic / elastic–plastic / viscoelastic with fractal statistics	Thermo-viscoelastic Maxwell-type
Thermal effects	Not considered (isothermal)	Explicitly included	Considered only partially (e.g., Persson)	Explicitly included and coupled
Surface roughness	None (smooth contact idealization)	None (smooth contact idealization)	Fractal or spectral representation (statistical, Weierstrass)	Fractal, nominally flat
Time-dependent creep	Considered (under monotonic loading)	Considered (thermo-viscoelastic creep)	Considered (rough-surface viscoelastic and hysteresis)	Considered (thermo-viscoelastic creep)
Analytical solution	Closed-form convolution integrals	Semi-analytical or numerical	Semi-analytical, series expansions, or approximations	Closed-form expressions (e.g., Equation 21)
Coupling load–temperature–deformation*	Not coupled	Fully coupled	Not coupled (partial in Persson)	Fully coupled
Experimental validation	Indentation and impact experiments	Polymeric contact and TVEHL tests	Friction and roughness measurements	Validation with Handzel-Powierza et al. [55]

Note: * "Load–Temperature–Deformation coupling" denotes whether the model explicitly accounts for the interaction between applied load, temperature effects (heating, temperature-dependent modulus), and the resulting deformation/creep response.

Table 2. Comparison of classical and proposed viscoelastic models for contact creep analysis

Model	Parameters (complexity)	Analytic tractability (creep/contact solutions)	Domain of validity (contact)	Accuracy / suitability	Remarks
Kelvin–Voigt	2 (E, η)	Very high (simple algebra)	Valid under monotonic contact but cannot capture relaxation	Poor for long-term creep; only instantaneous elasticity + linear creep	Overly stiff at short times, no stress relaxation
Maxwell	2 (E, η)	Moderate (closed forms available, diverges under sustained creep)	Monotonic loading (Radok admissible)	Good for long-term creep, poor short-term response	No instantaneous elasticity
Standard Linear Solid (SLS / Zener)	3 (E_1, E_2, η)	High (Laplace domain algebra manageable)	Monotonic loading (Radok admissible)	Captures both creep and relaxation, but limited flexibility	Balance between simplicity and realism
Fractional Maxwell	3 (E, η, α)	Moderate (involves Mittag–Leffler functions; analytic but less transparent) [66]	Same monotonic contact constraint, harder in closed solutions	High accuracy across wide time scales (power-law creep)	Flexible but less physically transparent, calibration can be difficult
Proposed Maxwell-based thermo-viscoelastic framework	2–3 (depending on thermal coupling)	High (explicit expressions, e.g., Equation 21; contact integrals remain tractable)	Extended beyond Radok monotonic requirement (generalized creep kernel)	Accurate under broad thermo-viscoelastic loading histories	Retains analytic clarity while extending applicability to thermo-mechanical contact problems

confined to elastic or elastic–plastic material laws, neglecting long-term creep. Experimental studies, for example by Handzel-Powierza et al. [55], highlighted the combined influence of surface roughness and time-dependent deformation in steels. Table 1 consolidates these perspectives, contrasting the assumptions, strengths, and limitations of the major modeling paradigms. Within this landscape, the present Maxwell-based thermo-viscoelastic framework offers a distinctive contribution by explicitly coupling load, temperature, and deformation, while retaining analytical tractability and enabling comparison with experimental creep data on rough surfaces.

To further clarify the scope and novelty of the present formulation, a comparative summary is provided in Table 2. This table contrasts the proposed Maxwell-based thermo-viscoelastic framework with commonly used viscoelastic models, including the Kelvin-Voigt, standard linear solid (SLS), and fractional Maxwell formulations. The comparison highlights the differences in accuracy relative to parameter complexity, analytic tractability (e.g., the availability of closed-form solutions such as Eq. 21), and the domain of validity, particularly with respect to Radok's monotonic contact restriction. As it was shown, the present framework achieves a favorable balance by explicitly capturing creep and thermo-mechanical coupling while maintaining analytical manageability, thereby offering the predictive capability that complements and extends the existing approaches.

CONCLUSIONS

In this research work, a novel fractal micro-contact model was presented to predict the asperity flattening under creep resulting from the temperature-dependent contact between a rough viscoelastic surface and a rigid flat surface. In order to realize the aforementioned objective, the constitutive equation was approximated using the Maxwell model and the interface topography in that model was simulated using fractal geometry. Moreover, the impact of temperature on creep has been investigated using Arrhenius' equation and the activation energy idea. Geometrically, the accuracy with which this model will simulate the creep deformation of a non-deterministic rough surface is debatable. This can be attributed to the Cantor set model's periodicity, resulting in geometrically uniform contact regions at each level of the structural hierarchy through the application of the same construction technique. Waviness and tortuosity at various scales are present in the real contact region of viscoelastic solid surfaces, according to tests; therefore, despite being utilized

to conduct an accurate analytical analysis of contact problem solutions, this model might not be overly detached from reality, i.e., the model does, however, admit an analytical solution.

In addition, the research demonstrated that a small and steady strain rate is often present during the secondary stage of creep. Since the traditional Maxwell model highlights the creep of a viscoelastic material to a first approximation and assumes linearity, it is predicted that it will not reflect the constant strain rate of the secondary stage, therefore a more sophisticated model is to be suggested In conclusion, the experimental data sourced from publicly available testing campaigns indicate that both the Cantor-based structural model and the Maxwell thermo-viscoelastic constitutive framework provide a robust and reliable representation of time-dependent material response under thermal and mechanical loading. The proposed model offers valuable insights into the influence of microstructural surface characteristics and constitutive behavior on creep deformation, and highlights the significance of various surface engineering techniques in governing subsequent deformation behavior. Furthermore, the field of contact mechanics and thermally driven creep continues to advance, reinforcing its critical role in the broader study of surface and interface phenomena. Future research in this area holds substantial potential to influence the related domains such as adhesive contact mechanics, the onset of sliding motion, and strain hardening mechanisms in tribological interfaces.

REFERENCES

1. Yang W. H., The contact problem for viscoelastic bodies, J Appl Mech, 1966; 33: 395–401.
2. Lee E. H. and Radok J. R. M., The contact problem for viscoelastic bodies, J. Appl. Mech., Sept. 1960; 27(3): 438–444, doi: 10.1115/1.3644020.
3. Jaffar M. J., Asymptotic behaviour of thin elastic layers bonded and unbonded to a rigid foundation, Int. J. Mech. Sci., 1989; 31(3): 229–235.
4. Whitehouse D. J. and Archard J. F., The properties of random surfaces of significance in their contact, Proc. R. Soc. Lond. Math. Phys. Sci., Mar. 1970; 316(1524): 97–121, doi: 10.1098/rspa.1970.0068.
5. Chang W. R., Etsion I., and Bogy D. B., An elastic-plastic model for the contact of rough surfaces, J. Tribol., Apr. 1987; 109(2): 257–263, doi: 10.1115/1.3261348.
6. Bush A. W., Gibson R. D., and Thomas T. R., The elastic contact of a rough surface, Wear, 1975; 35(1): 87–111.
7. Greenwood J. A. and Williamson J. B. P., Contact of nominally flat surfaces, Proc. R. Soc. Lond. Ser. Math. Phys. Sci., Dec. 1966; 295(1442): 300–319, doi: 10.1098/rspa.1966.0242.
8. Sayles R. S. and Thomas T. R., Computer simulation of the contact of rough surfaces, Wear, 1978; 49: 273–296.
9. Thomas T. R., Defining the microtopography of surfaces in thermal contact, wear, 1982; 79: 73–82.
10. Borodich F. M. and Mosolov A. B., Fractal roughness in contact problems, J. Appl. Math. Mech., 1992; 56(5): 681–690.
11. Chen J., Liu D., Wang C., Zhang W., and Zhu L., A fractal contact model of rough surfaces considering detailed multi-scale effects, Tribol. Int., 2022; 176: 107920.
12. Goerke D. and Willner K., Normal contact of fractal surfaces—experimental and numerical investigations, Wear, 2008; 264(7–8): 589–598.
13. Jackson R. L., An analytical solution to an archard-type fractal rough surface contact model, Tribol. Trans., July 2010; 53(4): 543–553, doi: 10.1080/10402000903502261.
14. Lan G., Sun W., Zhang X., Chen Y., Tan W., and Li X., A three-dimensional fractal model of the normal contact characteristics of two contacting rough surfaces, AIP Adv., 2021; 11(5), Accessed: Dec. 19, 2023. [Online]. Available: https://pubs.aip.org/aip/adv/article/11/5/055023/1036918
15. Majumdar A. and Bhushan B., Fractal model of elastic-plastic contact between rough surfaces, J Tribol., 1991; 113: 1–11.
16. Wang R., Zhu L., and Zhu C., Research on fractal model of normal contact stiffness for mechanical joint considering asperity interaction, Int. J. Mech. Sci., 2017; 134: 357–369.
17. Warren T. L., Majumdar A., and Krajcinovic D., A Fractal model for the rigid-perfectly plastic contact of rough surfaces, J Appl Mech, 1996; 63: 47–54.
18. Warren T. L. and Krajcinovic D., Fractal models of elastic-perfectly plastic contact of rough surfaces based on the Cantor set, Int. J. Solids Struct., Oct. 1995; 32(19): 2907–2922, doi: 10.1016/0020-7683(94)00241-N.
19. Kogut L. and Jackson R. L., A comparison of contact modeling utilizing statistical and fractal approaches, J. Tribol., Aug. 2005; 128(1): 213–217, doi: 10.1115/1.2114949.
20. Shen F., Li Y.-H., and Ke L.-L., A novel fractal contact model based on size distribution law, Int. J. Mech. Sci., July 2023; 249: 108255, doi: 10.1016/j.ijmecsci.2023.108255.
21. Xu K., Yuan Y., and Chen J., The effects of size distribution functions on contact between fractal rough surfaces, Aip Adv., 2018; 8(7): 075317.

22. Ling F. F., Fractals, engineering surfaces and tribology, Wear, 1990; 136(1): 141–156.
23. Liu S. H., Kaplan T., and Gray L. J., Theory of the AC response of rough interfaces, in Fractals in physics, Pietronero, L. and Tosatti, E.(editors), 1986; 383–389.
24. Shen J. and Wei W., Fractal characteristic and domain extension factor study on contact model of rough surface, Fractals, Dec. 2020; 28(8): 2040024, doi: 10.1142/S0218348X20400241.
25. Zhou A. A., Chen T., Wang X., and Xi Y., Fractal contact spot and its application in the contact model of isotropic surfaces, J. Appl. Phys., 2015; 118(16).
26. Zając K., Płatek K., Wachel P., and Łatka L., Fractal dimension as robust estimate of low carbon steels hardness, Adv. Sci. Technol. Res. J., 2022; 16(5), doi: 10.12913/22998624/155799.
27. Abuzeid O., Linear viscoelastic creep model for the contact of nominal flat surfaces based on fractal geometry: Maxwell type medium, Dirasat-Eng. Sci. Univ. Jordan, 2003; 30(1): 22–36.
28. Abuzeid O. M., A linear thermo-visco-elastic creep model for the contact of nominal flat surfaces based on fractal geometry: Kelvin-Voigt medium, J. Qual. Maint. Eng., 2003; 9(2): 202–216.
29. Abuzeid O. M., A linear viscoelastic creep-contact model of a flat fractal surface: Kelvin-Voigt medium, Ind. Lubr. Tribol., 2004; 56(6): 334–340.
30. Abuzeid O., A viscoelastic creep model for the contact of rough fractal surfaces: Jeffreys' type material, in Proceedings of the 7th International Conference Production Engineering and Design for Development, Ain Shams University, Cairo, Egypt., 2006.
31. Abuzeid O. M. and Eberhard P., Linear viscoelastic creep model for the contact of nominal flat surfaces based on fractal geometry: Standard linear solid (SLS) material, J. Tribol., Feb. 2007; 129(3): 461–466, doi: 10.1115/1.2736427.
32. Alabed T. A., Abuzeid O. M., and Barghash M., A linear viscoelastic relaxation-contact model of a flat fractal surface: a Maxwell-type medium, Int. J. Adv. Manuf. Technol., Nov. 2008; 39(5–6): 423–430, doi: 10.1007/s00170-007-1234-2.
33. Abuzeid O. M. and Alabed T. A., Mathematical modeling of the thermal relaxation of nominally flat surfaces in contact using fractal geometry: Maxwell type medium, Tribol. Int., 2009; 42(2): 206–212.
34. Abuzeid O. M., A novel hereditary viscoelastic Fractional-Fractal creep model for the contact of rough Surfaces: Maxwell medium, Ain Shams Eng. J., Aug. 2025; 16(8): 103458, doi: 10.1016/j.asej.2025.103458.
35. Li Q., Popov M., Dimaki A., Filippov A. E., Kürschner S., and Popov V. L., Friction between a viscoelastic body and a rigid surface with random self-affine roughness, Phys. Rev. Lett., July 2013, 111(3): 034301, doi: 10.1103/PhysRevLett.111.034301.
36. Carbone G. and Putignano C., Rough viscoelastic sliding contact: Theory and experiments, Phys. Rev. E, Mar. 2014; 89(3): 032408, doi: 10.1103/PhysRevE.89.032408.
37. Putignano C., Carbone G., and Dini D., Mechanics of rough contacts in elastic and viscoelastic thin layers, Int. J. Solids Struct., 2015; 69: 507–517.
38. Argatov I. I. and Popov V. L., Rebound indentation problem for a viscoelastic half-space and axisymmetric indenter — Solution by the method of dimensionality reduction, ZAMM - J. Appl. Math. Mech. Z. Für Angew. Math. Mech., Aug. 2016; 96(8): 956–967, doi: 10.1002/zamm.201500144.
39. Putignano C. and Carbone G., Viscoelastic Damping in alternate reciprocating contacts, Sci. Rep., 2017; 7(1): 8333.
40. Menga N., Afferrante L., Demelio G. P., and Carbone G., Rough contact of sliding viscoelastic layers: numerical calculations and theoretical predictions, Tribol. Int., 2018; 122: 67–75.
41. Putignano C., Menga N., Afferrante L., and Carbone G., Viscoelasticity induces anisotropy in contacts of rough solids, J. Mech. Phys. Solids, 2019; 129: 147–159.
42. Xie Y., Xiao Y., Lv J., Zhang Z., Zhou Y., and Xue Y., Influence of creep on preload relaxation of bolted composite joints: Modeling and numerical simulation, Compos. Struct., 2020; 245: 112332.
43. Jiang L., Wu M., Yu Q., Shan Y., and Zhang Y., Investigations on the adhesive contact behaviors between a viscoelastic stamp and a transferred element in microtransfer printing, Coatings, 2021; 11(10): 1201.
44. Putignano C. and Carbone G., On the role of roughness in the indentation of viscoelastic solids, Tribol. Lett., Dec. 2022; 70(4): 117, doi: 10.1007/s11249-022-01658-4.
45. Liang X.-M., Ding Y., Li C.-Y., and Wang G.-F., An incremental contact model for rough viscoelastic solids, Int. J. Mech. Sci., 2023; 255: 108483.
46. Tabaza T. A., Tabaza O., Barrett J., and Alsakarneh A., Hysteresis modeling of impact dynamics using artificial neural network, J. Mech., Jan. 2021; 37: 333–338, doi: 10.1093/jom/ufab007.
47. Abuzeid O. M., A novel hereditary viscoelastic Fractional-Fractal creep model for the contact of rough Surfaces: Maxwell medium, Ain Shams Eng. J., Aug. 2025; 16(8): 103458, doi: 10.1016/j.asej.2025.103458.
48. Mandelbrot B. B., The fractal geometry of nature, vol. 1. WH freeman New York, 1982.
49. Voss R., Fractals in nature: From characterization to simulation., in The Science of Fractal Images, H.-O. Peitgen,. and D. Saupe, (editors):, 1988; 21–70.
50. Johnson K. L., Contact Mechanics, vol. 1. Cambridge University Press, London., 1985.
51. Radok J. R. M., Viscoelastic stress analysis, Q. Appl Math, 1957; 15: 198–202.

52. Junisbekov T. M., Kestel′man V. N., and Malinin N. I., Stress relaxation in viscoelastic materials, Sci. Publ., 2003, Accessed: Dec. 19, 2023. [Online]. Available: https://cir.nii.ac.jp/crid/1130000797374086016
53. Boyle J. T. and Spence J., Stress analysis for creep. Elsevier Ltd., 1983.
54. Lee W.-S. and Liu C.-Y., The effects of temperature and strain rate on the dynamic flow behaviour of different steels, Mater. Sci. Eng. A, 2006; 426(1–2): 101–113.
55. Handzel-Powierza Z., Klimczak T., and Polijaniuk A., On the experimental verification of the Greenwood-Williamson model for the contact of rough surfaces, Wear, 1992; 154(1): 115–124.
56. Bland D. R., The theory of linear viscoelasticity. Pergamon Press, Belfast, 1960.
57. Shames I. H. and Cozzarelli F. A., Elastic and Inelastic Stress Analysis. CRC Press, Boca Raton, Florida., 1992.
58. Ting T. C. T., The contact stresses between a rigid indenter and a viscoelastic half-space, J. Appl. Mech., Dec. 1966; 33(4): 845–854, doi: 10.1115/1.3625192.
59. Roberts G. E. and Kaufman H., Table of Laplace Transforms. Philadelphia: W.B. Saunders Company, 1966.
60. Slater L. J., Confluent Hypergeometric Functions. London: Cambridge University Press, 1960.
61. Hunter S. C. The Hertz problem for a rigid spherical indenter and a viscoelastic half-space, J. Mech. Phys. Solids, Nov. 1960; 8(4): 219–234, doi: 10.1016/0022-5096(60)90028-4.
62. He T. et al., Modeling thermal-visco-elastohydrodynamic lubrication (TVEHL) interfaces of polymer-based materials, Tribol. Int., Feb. 2021; 154: 106691, doi: 10.1016/j.triboint.2020.106691.
63. Zhang X. et al., Fully coupled thermo-viscoelastic (TVE) contact modeling of layered materials considering frictional and viscoelastic heating, Tribol. Int., June 2022; 170: 107506, doi: 10.1016/j.triboint.2022.107506.
64. Persson B. N. J., Theory of rubber friction and contact mechanics, J. Chem. Phys., Aug. 2001; 115(8): 3840–3861, doi: 10.1063/1.1388626.
65. Ciavarella M., Demelio G., Barber J. R., and Jang Y. H., Linear elastic contact of the Weierstrass profile†, Proc. R. Soc. Lond. Ser. Math. Phys. Eng. Sci., Feb. 2000; 456(1994): 387–405, doi: 10.1098/rspa.2000.0522.
66. Mainardi F., Fractional Calculus And Waves In Linear Viscoelasticity: An Introduction To Mathematical Models (Second Edition). World Scientific, 2022.